Biophysical Chemistry 135 (2008) 59–68

Contents lists available at ScienceDirect

Biophysical Chemistry

journal homepage: http://www.elsevier.com/locate/biophyschem

Cell-based screening for membranal and cytoplasmatic markers using dielectric spectroscopy

Amit Ron [a,*], Ragini Raj Singh [a], Nick Fishelson [a], Irena Shur [b], Rina Socher [b], Dafna Benayahu [b], Yosi Shacham-Diamand [a]

[a] Department of Electrical Engineering, Faculty of Engineering, Tel-Aviv University, Israel
[b] Department of Cell and Developmental Biology, Sackler Faculty of Medicine, Tel-Aviv University, Israel

ARTICLE INFO

Article history:
Received 24 February 2008
Received in revised form 16 March 2008
Accepted 16 March 2008
Available online 29 March 2008

Keywords:
Dielectric spectroscopy
Interfacial polarization
Cell screening
Lectin
SEC13

ABSTRACT

Dielectric spectroscopy (DS) of living biological cells is based on the analysis of the complex dielectric permittivity of cells suspended in a physiological medium. It provides knowledge on the polarization–relaxation response of cells to external electric field as function of the excitation frequency. This response is strongly affected by both structural and molecular properties of cells and therefore, can reveal rare insights on cell physiology and behaviour. This study demonstrates the mapping potential of DS after cytoplasmatic and membranal markers for cell-based screening analysis. The effect of membrane permittivity and cytoplasm conductivity was examined using tagged *MBA* and *MDCK* cell lines respectively. Comparing the permittivity spectra of tagged and native cell lines reveals clear differences between the analyzed suspensions. In addition, differences on the matching dielectric properties of cells were obtained. Those findings support the high distinction resolution and sensitivity of DS after fine molecular and cellular changes, and hence, highlight the high potential of DS as non invasive screening tool in cell biology research.

1. Introduction

The dielectric properties of biological cells can provide rare insight about the cellular and molecular state of given cells. Dielectric study of biological cells was explored for the first time by Hoeber, who investigated the dielectric properties of *Erythrocytes* [1]. Here the cells were characterized as poorly conducting membrane enclosing a conducting and polar cytoplasm. The foundations of understanding the dispersion mechanism of biological cells suspended in physiological medium have been suggested by Schwan according to the theories of mixed dielectrics, founded by *Maxwell & Wagner* [2,3]. Since then, the dielectric properties of many cell types have been explored by a number of authors [4–7].

Dielectric properties of biological cells are mainly characterized by β dispersion mechanism which accounted for the medium (MF) and high (HF) range of the radio spectrum [7,8]. This mechanism is due to *Maxwell–Wagner* effect (interfacial polarization) at the external and internal interfaces of the phospholipids membrane [9,10]. In addition, contribution may also arise from dispersion of small intra cellular organelles, which usually appear as small adjunct to the β dispersion at high frequencies.

Dielectric spectroscopy (DS) techniques can provide comprehensive knowledge about cell structure and properties, intra cellular content, membrane shape and selectivity and many more [11–13]. Using dynamic dielectric spectroscopy allows real time quantification of cellular and molecular processes occurring in cells during variety of biological mechanisms like: growth, activity, division etc. [14–18].

Recent interests in the development of new high throughput, non destructive screening techniques are largely driven by the potential for associating physical methods with cell and molecular biology methodologies. Cell-based screening is a powerful method that uses living cells to test the effect of different molecules like drugs and toxicants on the cellular and molecular phenotype of cells. This technique requires the use of high sensitive tools that permit high speed systematic identification of biochemical targets and markers on given cell libraries.

This study is aiming to demonstrate the use of DS as potential screening tool after bio-markers in cell-based screening analysis. This approach can offer label/mediator-free strategy for rapid analysis and monitoring of cellular and molecular markers in living cells. It can provide fast and reliable prediction on the viability and physiology of cells as response to induced chemical stimulations or can be used to monitor development and transformation processes occurring in the cell within its life cycle. In order to understand the practicable impact of it, it is first essential to understand the more fundamental research of membranal and cytoplasmatic tagging effect.

Madin-Darby Canine Kidney Epithelial (MDCK) and *Bone Marrow derived Pre-Osteoblastic (MBA)* cell lines were used to investigate the

* Corresponding author. Tel.: +972 3 6406946; fax: +972 3 6423508.
E-mail address: amitron@eng.tau.ac.il (A. Ron).

0301-4622/$ – see front matter © 2008 Elsevier B.V. All rights reserved.
doi:10.1016/j.bpc.2008.03.003

effectiveness of DS to follow intra cellular and membranal markers. The intra-cellular marker used was based on *SEC13* protein over-expressing *MDCK* cells. Effect of membrane was tested in *lectin*-labeled *MBA* cells that bind glycosylate elements on cell surface. The analyzed dielectric spectra confirm the modulation of both markers on the dielectric parameters of cells. Cytoplasm conductivity of *SEC13* over expressed and membrane permittivity of *MBA* coated cells were found to be affected when compared to the native cell lines. Those findings provide the necessary knowledge regarding the ability to correlate between molecular and cellular markers, and changes on the matching complex permittivity spectra and parameters of the cells.

2. Modeling the dielectric response of cells

Analysis of dielectric parameters depends on cell topography; therefore, a matched electric model should be applied based on those geometrical characteristics. Most biological cells can be treated as thin insulating shelled component (membrane) enclosing conducting medium (cytoplasm). This simple description brought many theories and models developed by several authors. The first model of shelled-spheroid was introduced by Frick [19], later it was extended to the case of shelled-ellipsoid particles [20]. Those models however, were limited to low frequencies analysis. Since then, several models were proposed by Pauly and Schwan [21], Hanai et al. [22], and Redwood et al. [23]. The first comprehensive model was introduced by Asami and Hanai, who for the first time presented unlimited approach for dielectric analysis of suspended shelled-ellipsoids [24].

Both *MBA* and *MDCK* cells exhibit an approximate elliptic structure (Fig. 1), and therefore, can be treated using the dispersed shelled-ellipsoids analysis. Here the cells are described as two phase systems (membrane and cytoplasm) surrounded by infinite and continues medium (Fig. 2). Based on the theory of interfacial polarization, the complex relative permittivity of dispersed shelled-ellipsoids ε^*, suspended in a medium with complex relative permittivity ε_m^*, is given by:

$$\varepsilon^* = \varepsilon_m^* + \frac{\Phi}{3}\sum_{k=x,y,z}\frac{\bar{\varepsilon}_m^*\left(\varepsilon_{ck}^* - \varepsilon_m^*\right)}{\bar{\varepsilon}_m^* + \left(\varepsilon_{ck}^* - \bar{\varepsilon}_m^*\right)L_k} \tag{1}$$

Where $\Phi = \frac{4\pi R_x R_y R_z N}{3}$ is the volume fraction of the cells and ε_{ck}^* is the complex relative permittivity of the shelled-ellipsoid across the k axis, given by:

$$\varepsilon_{ck}^* = \varepsilon_{om}^*\left(1 + \frac{v\left(\varepsilon_i^* - \varepsilon_{om}^*\right)}{\varepsilon_{om}^* + \left(\varepsilon_i^* - \varepsilon_{om}^*\right)L_{ik} - \left(\varepsilon_i^* - \varepsilon_{om}^*\right)vL_k}\right) \tag{2}$$

Where ε_{om}^*, ε_i^* are the complex relative permittivities of the membrane and cytoplasm respectively and v is the volume ratio given by:

$$v = \frac{R_{ix}\cdot R_{iy}\cdot R_{iz}}{\left(R_{ix} + \Delta_L\right)\left(R_{iy} + \Delta_L\right)\left(R_{iz} + \Delta_L\right)} \tag{3}$$

Δ_L is the membrane thickness and L_k, L_{ik} (k=x, y, z) are the depolarization factors, given by:

$$L_k = \frac{R_x R_y R_z}{2}\int_0^\infty \frac{ds}{\left(R_k^2 + s\right)\sqrt{\left(R_x^2 + s\right)\left(R_y^2 + s\right)\left(R_z^2 + s\right)}} \tag{4}$$

$$L_{ik} = \frac{R_{ix} R_{iy} R_{iz}}{2}\int_0^\infty \frac{ds}{\left(R_{ik}^2 + s\right)\sqrt{\left(R_{ix}^2 + s\right)\left(R_{iy}^2 + s\right)\left(R_{iz}^2 + s\right)}} \tag{5}$$

Where R_x, R_y, R_z and R_{ix}, R_{iy}, R_{iz} are the semi-axes of the cell and cytoplasm respectively.

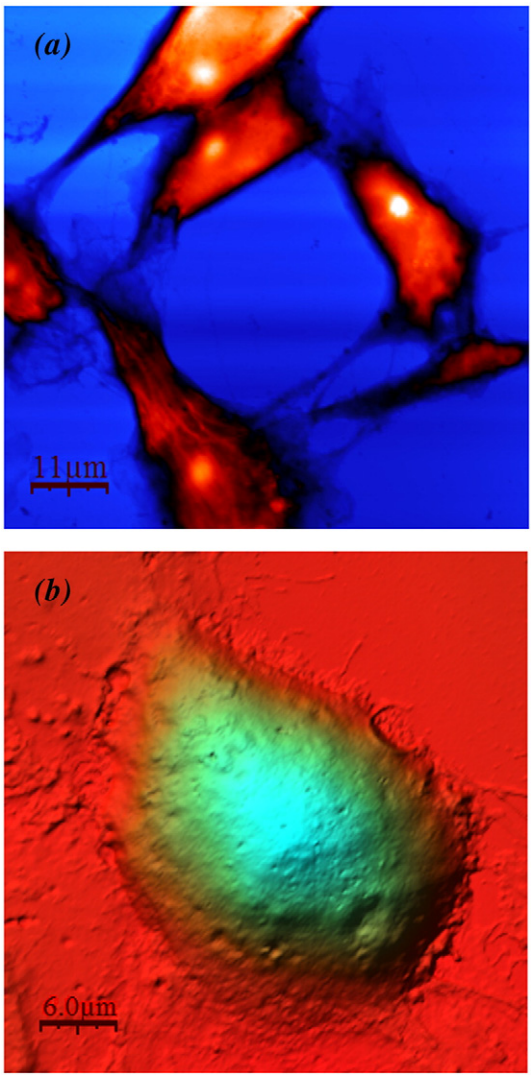

Fig. 1. Topographic images of cells. (a) Topography of joined *MBA* cells (70 μm×70 μm). (b) Topography of single *MDCK* cell (40 μm×40 μm). Both images recorded in physiological conditions in DMEM solution.

The medium relative permittivity is represented by the average value $\bar{\varepsilon}_m^*$. It can be found within the range of $\varepsilon_m^* \le \bar{\varepsilon}_m^* \le \varepsilon^*$, when it depends on cells concentration. At low concentration, the medium around each cell is assumed to be homogenous (cell free), and therefore, $\bar{\varepsilon}_m^* = \varepsilon_m^*$. When the cells concentration is high, each single cell surrounded by a mixture of cells and medium, and therefore, $\bar{\varepsilon}_m^* \approx \varepsilon^*$.

3. Methods

3.1. Preparation and analysis of cells

3.1.1. Cell cultures

Madin–Darby Canine Kidney Epithelial (*MDCK*) wild type or stable transfected with *SEC13*-GFP [25]. *MBA-15* cells are marrow stroma derived osteoprogenitors [26]. Cells were cultured in growth medium Dulbecco's Modified Essential Medium (DMEM) supplemented with 10% heat-inactivated fetal calf serum (FCS), 1% glutamine and 1% antibiotics, and maintained in 5% CO_2 at 37 °C.

3.1.2. Fluorescence-activated cell sorter (FACS)

Binding of *biotinylated-lectin Helix pomatia* (*HPA*, Sigma) to cell surface carbohydrate residues expression were analyzed by FACS. For

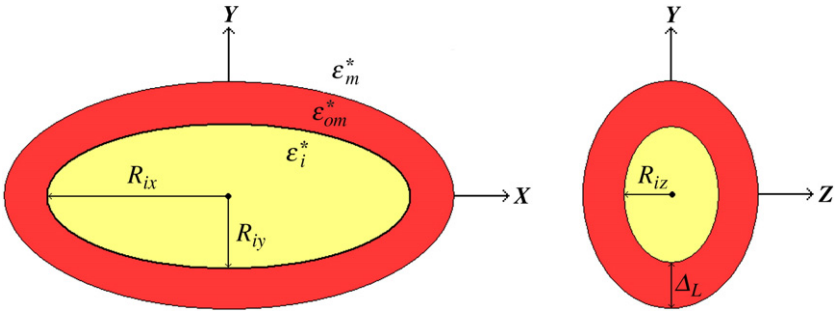

Fig. 2. Shelled ellipsoid model. *X–Y* plane (left), *Y–Z* plane (right). ε_m^*, ε_{om}^*, ε_i^* represent the complex permittivity of medium, membrane (red) and cytoplasm (yellow) respectively.

analysis adherent cells were released from culture using 0.5 mM EDTA in PBS. Single cell suspensions were blocking buffer, PBS containing 1% FCS, then cells were incubated for 30 min on ice with *HPA-biotin* conjugate and stained with Extravidine-FITC (Sigma). 10^4 cells were collected by FACS, and statistical analysis was performed using software from Becton Dickinson as described earlier [27].

FACS analysis of *MBA-15* cells revealed binding of *HPA* to cell membrane. Histogram (Fig. 3a) demonstrates 85% of cells that are stained with *HPA*. The intensity of cell staining versus cells size is shown by dot plots (Fig. 3b). This plot indicates the homogeneity of the tested suspension based on the forward scatter (FSC) of each cell. The obtained results indicate that the tagged suspension (*HPA+*) is homogenous, and therefore, confirm the *lectin* tagging on cells membrane.

3.1.3. Fluorescent microscopy observations

The *MDCK*-GFP-transfected cells were observed with inverted fluorescent microscope (Zeiss, Axiovert 200M, Germany). Images were acquired with an Axiocam MRm monochrome CCD camera. The CCD camera drive and color acquisition were controlled by Axiovision 4.4 imaging system, composites of digitized images were assembled using Adobe.

Stable transfected *MDCK* with *SEC13*-GFP are seen by fluorescence microscope. The over expressing of *SEC13* is distributed through the cytoplasm (Fig. 3c).

3.1.4. AFM analysis

The morphological parameters of cells were measured using Atomic Force Microscopy (Pico SPM II, Molecular Imaging). Topography (Fig. 1) of both *MBA* and *MDCK* cells was recorded on contact mode using Silicon nitride tips (Veeco NP-series, k=0.06 N/m). Force setpoint was taken to be 5 nN with scan rate of 0.4 lines/s. Cells were imaged in physiological conditions in specific fluid cell that covered with 200 µl of the cell serum (growth medium). Several cells were then analyzed in order to obtain their average geometrical dimensions.

Cross-section analysis revealed information about the average dimensions of *MBA* and *MDCK* cells respectively:

Average length (central axis): 24 µm, 26 µm.
Average width (central axis): 10 µm, 18 µm.
Average height (central axis): 1.2 µm, 1.6 µm.

3.2. Preparation of Pt black electrodes

Preparation of electrodes is based on procedure reported before [28], the procedure was slightly modified. Platinum black electrodes were cathodically electrodeposited on gold (Au) coated titanium (Ti) electrodes from an aqueous acidic bath. At first step gold was deposited on the titanium electrodes. Prior to the gold deposition the titanium electrodes were degreased in boiling isopropanol for 5 min and rinsed with de-ionized (DI) water. Degreased electrodes were etched chemically in fresh hot H_2SO_4 aqueous solution (50% by volume) for 5 s Following etching the electrodes were thoroughly rinsed in DI water and immediately transferred in the bath of gold electrodeposition. Electrodeposition was made in galvanostatic regime and the regular DC power supply was used.

The electrodeposition of gold was performed cathodically in galvanostatic conditions; the Enthone sulfite bath was used for the electrodeposition of gold. The cathode current density was 4 mA/cm^2 (titanium electrode) and anode current density was less than 2.5 mA/cm^2 (platinum (Pt) or Pt/Ti anodes). Anodes and cathodes were held in position to provide uniform current distribution over the cathode surface. Temperature of bath maintained at 50±1 °C with the help of temperature controller. During the electrodeposition the electrolyte was continuously stirred at a moderate speed with the help of a magnetic stir and Teflon coated paddle. The duration for Au electrodeposition was 20 min to obtain compact 5 µm thick layer of Au. At the end of the deposition, the electrode was quickly removed from the bath and was thoroughly cleaned with DI water and stored in the DI water prior to the platinum black plating.

For the deposition of platinum black on the gold deposited titanium electrode, the electrode was immersed in the 2% H_2PtCl_6 aqueous solution (this bath doesn't contain any other component). The current density was 5 mA/cm^2, Au/Ti electrode was used as cathode and Pt plate was used as anode. Anodes and cathodes were held in position to provide uniform current distribution over the cathode surface. Deposition lasts for 30 min to obtain 1 µm thick (2 mg/cm^2) porous Pt. This deposition was performed at room temperature and also there was no stirring required. After the deposition, the electrode was quickly removed from the bath and was thoroughly rinsed with DI water to remove the traces of solvent. The electrodes stored short-circuited in DI water till use.

3.3. Dielectric measurements

Dielectric measurements of cell suspensions were carried out over a frequency range of 100 Hz up to 100 MHz using 4294A Precision Impedance Analyzer (Agilent tech.). All measurements were carried out using Teflon cell, total volume of 750 µl using oblong parallel-plate Pt black coated electrodes with the following dimensions: d (electrodes separation)=5 mm, w (electrode width)=15 mm, h (electrode height)=10 mm and t (electrode thickness)=1 mm.

Since the parallel-plate condenser is finite in area, fringing effects are formed on the edges which can cause to the appearance of stray capacitance on the edges and consequently the measured capacitance can be larger than the capacitance of the dielectric sample. In order to minimize the fringing effect, all dielectric measurements were based on the three-terminal method [29]. Guard electrodes (2 mm in width) separated by 0.5 mm Teflon spacer were used beside the working electrode (guarded electrode), both the working and guard electrodes were held under the same potential against the counter electrode. The

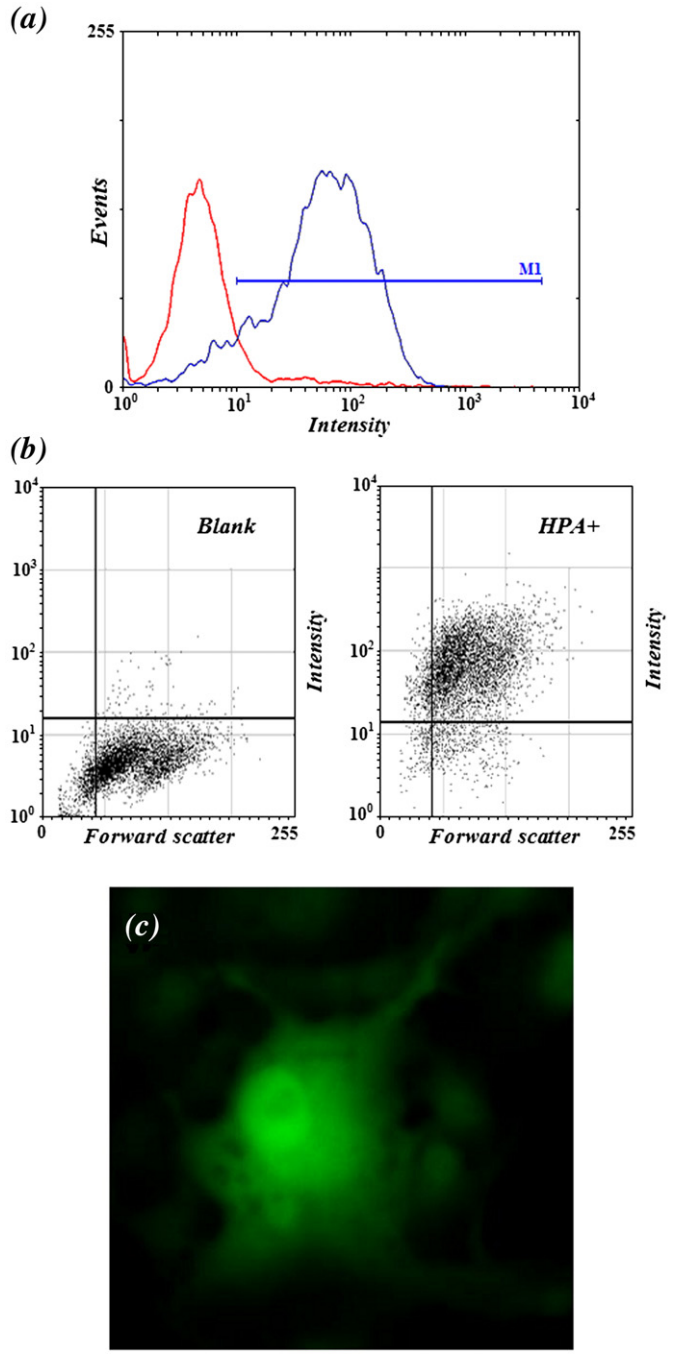

Fig. 3. FACS and immunofluorescence analysis. (a) Quantifying FACS data, the level of fluorescence intensity is given by the *X* axis; the number of cells is given by the *Y* axis. (b) Dot plot of *lectin* coated cells (*HPA+)* and untagged cells (*Blank*). The level of fluorescence intensity is given by the *Y* axis; the relative size of cells is represented by the forward scatter signal and given by the *X* axis. (c) Immunofluoresnce image of *MDCK* cell which transfected by GFP-*SEC13* protein.

given configuration provides a parallel field between the working and counter electrodes. The guard electrodes absorb the electric field at the edge and the measured capacitance between the electrodes is only composed of the current that flows through the dielectric sample. In addition, in order to avoid gap capacitances, tightening screws were used to place the electrodes tight to the Teflon walls. The measured air capacitance was then found to be 0.26 pF.

The Teflon cell was cleaned before each measurement using Piranha (1:3, 30% H_2O_2, 96% H_2SO_4) during 20 min. This ensured removal of adsorbed organic material from the cell walls. Cleaning of Pt black electrodes was performed in 1 M H_2SO_4 by passing cathodic current, 10 mA/cm^2 during 1 min.

The durability of Pt black electrodes was tested before each measurement in order to avoid degradation of the platinum black which deteriorates with sequential use. The polarization capacitance of unused Pt black electrode in 1 M H_2SO_4 was found to be 24 mF/cm^2 (using *C–V* method in double layer region, ν=50 mV/s); the roughness factor (surface increase coefficient) was 185. When the polarization capacitance was found to be significantly lower than this value (approximately 5 times), the electrodes were replaced.

The suspension medium was evaluated before each measurement for both conductivity and permittivity. Cells at specific concentration were filtered out from the growth medium and then suspended again in a fresh medium (total volume of 750 µl) before the beginning of each measurement. All measurements were performed at room temperature (25 °C); evolution of measurements is summarized using Table 1. The measured data was corrected for leads/cell inductance and polarization impedance (Section 3.4). In addition, non linearity of current was checked to avoid errors in correction of polarization impedance which can have large impact on the measured data (Section 3.4).

The measured dielectric spectrum was extracted from the corrected impedance data using an equivalent electric circuit (Fig. 4). Here $C_m = C_0(\varepsilon' - j\varepsilon'')$ is the complex capacitance of the suspension and R_m represents the leakage current through the capacitor (dc con ductivity).

3.4. Linearity effect and impedance corrections

The polarization impedance is independent of the current densities only for small current densities. This phenomenon is critical mainly in high conductive samples and on low frequencies [30]. Here linearity of the impedance versus current density was checked for platinum black electrodes (~0.7 cm^2), against large reference, in DMEM solution for frequency range from 100 Hz up to 1 kHz (Fig. 5a, b).

The results indicate on a limit density of 0.6 mA/cm^2 at low frequencies, up to 2.4 mA/cm^2 at 1 kHz. It means that limit of linearity shifts to higher current densities as the frequency is increased. Based on those results, the applied voltage should be set for <200 mV (100 mV was applied in all measurements) in order to avoid non-linear affects which introduce significant errors on the measured impedance signal.

Electrode polarization was corrected for both resistance and capacitance effects (Fig. 5c) based on a procedure suggested before [31]. Here polarization capacitance (C_L) and resistance (R_L) are given by:

$$\frac{1}{C\omega} = \left(1 + \frac{1}{(RC\omega)^2}\right) \cdot \left(\frac{1}{C_L\omega} + \frac{R_m^2 C_m \omega}{(R_m C_m \omega)^2 + 1}\right) \quad (6)$$

$$R = \left(1 + (RC\omega)^2\right) \cdot \left(R_L + \frac{R_m}{1 + (R_m C_m \omega)^2}\right) \quad (7)$$

Where R_m is the sample resistance, C_m is the sample capacitance; *R* and *C* are the measured parameters of the sample. Based on the low

Table 1
Measurement characteristics of cell suspensions

Cell	Volume fraction	Number of samples	Recorded cycles
MBA	0.03	3	2
MBA-lectin	0.03	3	2
MDCK	0.05	3	2
MDCK-SEC13	0.05	3	2

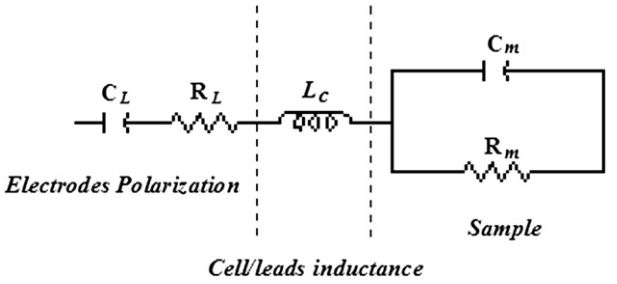

Fig. 4. Equivalent electrical circuit. The sample is represented by parallel capacitor (C_m) and resistor (R_m) which stand for permittivity and conductivity respectively. The effect of cell/leads inductance and polarization impedance is modelled by inducer (L_c) and resistor–capacitor (R_L, C_L) elements in series with the sample.

volume fraction of cells, the shielding effect caused by the cells is negligible, and therefore, the reliability of this correction technique is high [32].

Inductance of leads/capacitor was evaluated at high frequency (1 MHz) when the measured impedance is free from polarization effects (Fig. 5d) [33]. Here the sample capacitance was measured as function of sample conductivity (electrolyte concentration). The inductance is then calculated as the slope of the obtained curve, when:

$$L_c = -\frac{dC_m}{dR_m^{-2}} \tag{8}$$

4. Results

Based on the topography of *MBA* and *MDCK* cells (Fig. 1), both of them can be approximated as single-shell ellipsoids. Here the cytoplasm is bound by a membrane of finite thickness d, with inner dimensions R_{ix}, R_{iy}, R_{iz}. This simple model of the cell is already proved as very effective in following after cellular phenotypes [15,16]. At screening analysis, this model can be very useful to predict general changes occurring in both phases of the cell without to take into account the specific contribution of each internal organelle. It means that the net change of the cell is observed instead of many local changes.

The interface (phospholipids membrane), that separates the different dielectric layers, introduces two possible dispersion mechanisms caused by both conductivity and permittivity differences between the cytoplasm and the exterior medium. When multiple

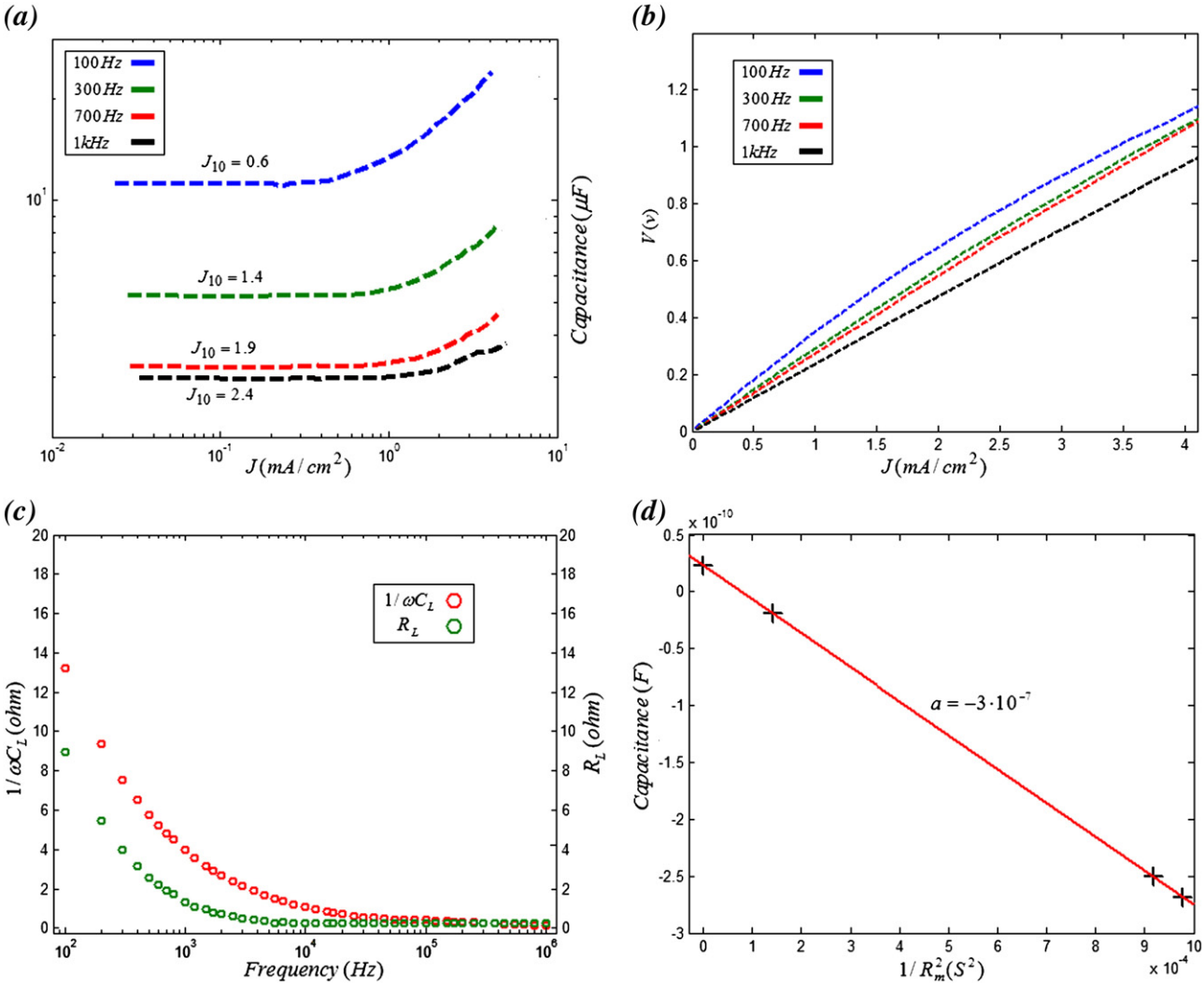

Fig. 5. Pt black electrodes and inductance characteristics. (a) Voltage versus current density at 100, 300, 700 and 1000 Hz. The limit of linearity is continuously increased with frequency. (b) Polarization capacitance versus current density at 100, 300, 700 and 1000 Hz. J_{10} indicates the current density at 10% deviation from linearity. (c) Effect of polarization impedance as function of frequency. The impedance is exponentially fades as the frequency increase. (d) Apparent capacitance as function of medium resistivity. The inductance is extracted as the slope of the obtained curve. Measurements were performed in high frequency (1 MHz) to avoid electrodes polarization affect.

dispersions exist, each is activated by different mechanism, and therefore, takes place at specific frequency range. Here the dispersion mechanism accounted to *Maxwell–Wagner* effect is expected to be most sensitive to changes related to permittivity and conductivity of the membrane and the cytoplasm respectively. It means that the induced dipole, and hence the complex dielectric spectrum, are expected to be strongly dependent on the electrical properties of both membrane and cytoplasm.

Based on the dielectric properties of cells, the cytoplasm conductivity and the membrane permittivity should be influenced by molecular changes occur on those phases respectively. Here *MBA* and *MDCK* cell lines have been subjected to dielectric spectroscopy. In addition, treated cell lines of both strains (*MBA-lectin* coated, *MDCK-SEC13*) were investigated and compared to the untreated cells.

The obtained dielectric spectra of cells are given in Fig. 6. All measurements indicate on dispersion mechanism which is accounted

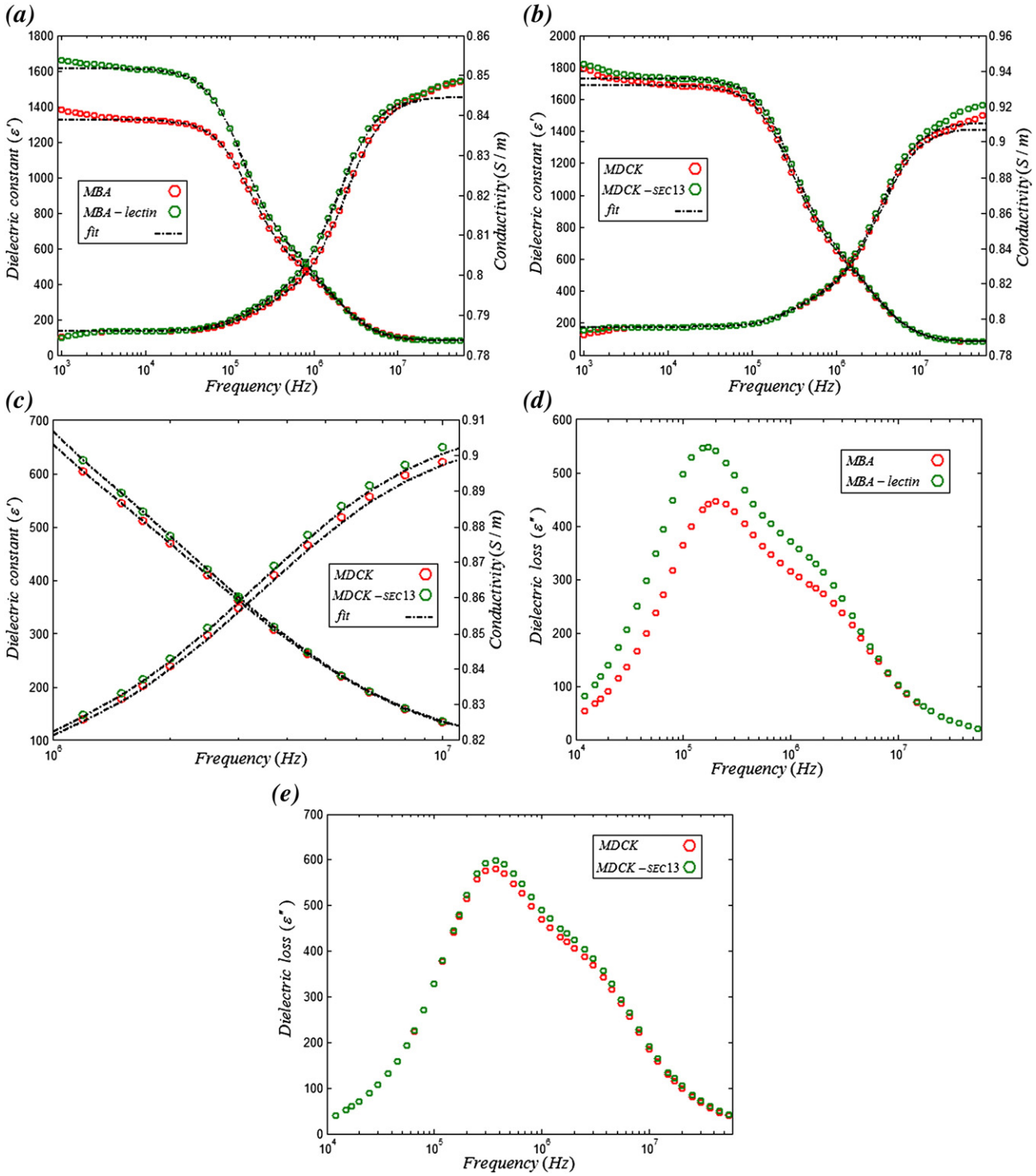

Fig. 6. Dielectric spectra of *MBA* and *MDCK* cell suspensions (based on the average of all 6 measurements). (a) Dielectric and conductivity spectra of *MBA* and *MBA-lectin* suspensions. (b) Dielectric and conductivity spectra of *MDCK* and *MDCK-SEC13* suspensions. (c) High frequency observation on *MDCK* and *MDCK-SEC13* spectra. (d) Loss spectra of *MBA* and *MBA-lectin* suspensions. (e) Loss spectra of *MDCK* and *MDCK-SEC13* suspensions.

for the *Maxwell–Wagner* effect (interfacial polarization). Additionally, sub dispersions are obtained which resulted from large variation of the depolarization factors along the three axes. The deviation of dielectric values around 1 kHz is related to the effect of electrode polarization which cannot be corrected completely. The steep rise on conductivity values at high frequencies is related to contribution of additional dispersion mechanism which probably related to molecular relaxation and dispersion of internal organelles within the cell. Those usually appear as small adjunct to the β dispersion at high frequencies as obtained by the measured spectra.

Comparing the complex dielectric spectra of *MBA WT* (*Wild Type*, untreated cells) cells and the *lectin* coated cells (Fig. 6a), reveals clear differences between those two cell lines. The obtained permittivity (ε') of the treated cells is found to be higher than the *WT* cells. This rise is expected due to the presence of charged groups on the membrane, which affect its capacitive part. Additionally, based on the dielectric loss (ε'') spectrum (Fig. 6d), changes are also obtained on the frequency dispersion characteristic. Here the loss factor is shifted to lower frequencies due to the increase in membrane permittivity and hence its capacitance. This was caused due to the increase on medium-membrane charge relaxation time ($\tau_{\text{med-mem}} \approx \varepsilon_{\text{mem}}/\sigma_{\text{med}}$) which directly affects the relaxation time of the whole medium-cell system.

The obtained *MDCK* spectra (Fig. 6b, c), demonstrate meaningful differences at relatively high frequencies when charge and ion migration (conductive polarization) start to fade. This happens when the frequency exceeds the inverse relaxation time of the medium-membrane interface. Here the *SEC13* cells exhibit higher dispersion characteristics comparing to the *WT* cells. This caused by changes occurred in cytoplasm conductivity which affected the cytoplasm-medium relaxation time ($\tau_{\text{cyt-med}} \approx \varepsilon_{\text{med}}/\sigma_{\text{cyt}}$). The characteristic frequency of cells ($1/\tau$) is now increasing due to the increase in cytoplasm conductivity.

In order to estimate the exact dielectric parameters of cells, the mixed dielectric equation (Eq. (1)) was fitted to the experimental data (Fig. 6a–c, broken line). Phase parameters were extracted based on a well known procedure suggested before and efficiency used by several authors [24,34]. In order to minimize the error between the measured and fitted data, the residuals between the two curves were minimized using means error function given by Eq. (9).

$$M(\varepsilon,\sigma) = \sqrt{\frac{\sum_j \left(\hat{\varepsilon}_j - \bar{\varepsilon}_j\right)^2}{\sum_j \bar{\varepsilon}_j^2} + \frac{\sum_j \left(\hat{\sigma}_j - \bar{\sigma}_j\right)^2}{\sum_j \bar{\sigma}_j^2}} \tag{9}$$

Where $\hat{\varepsilon},\hat{\sigma}$ are the fitted permittivity and conductivity respectively and $\bar{\varepsilon},\bar{\sigma}$ are the measured permittivity and conductivity of the suspension, where *j* stands for the excitation frequency. All phase parameters have been evaluated based on the average values of 6 measurements for each cell type. Additionally, the membrane conductivity which is very low, especially in non-excitable cells [35], was neglected and assumed to have no effect on the obtained spectra. The thickness of *MDCK* and *MBA* membranes was taken to be 6 nm [36,37]. The fitted parameters are summarized in Table 2.

The obtained phase parameters indeed indicate on clear changes between both *WT* cell lines and their mutants. All deviations are found to be approximately ±5% from the mean value which is a reasonable and acceptable value. In addition, all phase parameters exhibit similar deviation when comparing the tagged and native cells. It means that the deviation is consistent with the measurement and hence, didn't affect the distinction ratio between parallel phase parameters of tagged and native cells.

As expected, the membrane capacitance of *lectin* tagged *MBA* cells found to be higher then the *WT* cells. In addition, small changes in cytoplasm conductivity and permittivity are noticed; those may be related to sub structural or molecular changes caused by the *lectin* binding. The phase parameters of *MDCK* cell lines indicate on clear difference in cytoplasm conductivity between *WT* and treated cell lines. This change is related to the over expression of *SEC13* protein. The small change in cytoplasm permittivity may be attributed to the polarization characteristics of this protein which is additive to the total dielectric polarization ($\varepsilon'_{\text{cyt}}$) of the cytoplasm.

Table 2
Dielectric characteristics of native and treated cell lines

Cell	ε_{m}	σ_{m} (ms/cm)	ε_{om}	C_{mem}(μF/cm)	ε_i	σ_i(ms/cm)
MBA	81	8.5	6.11±0.5	0.9±0.07	68±4	7.24±0.5
MBA-lectin	81	8.5	7.53±0.4	1.11±0.06	67±4	7.12±0.4
MDCK	84	9.1	4.72±0.6	0.69±0.09	70±2	9.3±0.4
MDCK-SEC13	84	9.1	4.85±0.5	0.71±0.07	73±3	9.98±0.4

All parameters are given as mean ± standard deviation except of medium permittivity and conductivity which evaluated separately before each measurement.

The affect of membrane conductivity was evaluated separately in order to avoid errors in the fitted parameters. Phase parameters found to be independent of membrane conductivity up to values of ~10^{-5} S/m. When membrane conductivity was increased, major changes were obtained on membrane permittivity (ε_{om}). Those changes however, didn't affect the ratio between parallel phase parameters of *WT*, and treated cell lines, on both cell types. It means that membrane conductivity, can only fundamentally affect membrane permittivity. If the conductivity is low (low ion channels activity), then it behaves like a pure dielectric membrane with large capacitance values. Otherwise, when the conductivity is significant (high ion channels activity), the membrane is partially lumped with the cytoplasm and hence, reduces the effective influence of membrane as isolating shell.

5. Discussion

This study is aiming to demonstrate the use of DS as screening tool after cellular and molecular markers. The screening ability of fine differences on membrane permittivity, and cytoplasm conductivity, has been demonstrated using *MBA* and *MDCK* cells respectively. The analysis is based on comparison of differences in intra cellular proteins using *MDCK* over-expressing *SEC13* and membrane binding of *lectin* on cell surface of *MBA* cells. The observed dielectric spectra allow clear distinction between treated and untreated cell lines and hence, confirm the applied biological modification on both treated cell lines. Moreover, based on previous studies of mammalian cells, all phase parameters are found to be within reasonable range for both membrane and cytoplasm components [5,17,38]. This comparison, even for different cell types, can provide to some extent indication on both accuracy and reliability of the measured and fitted data.

The single-shell model is found to be very useful in the presented screening analysis. Average changes, occurring in both phases of the cell, have been probed successfully without taking into account specific contribution of internal organelles. Meaning that the net change of the cells was observed instead of many local changes. Therefore, the use of the two phase model can be very useful to predict average changes rather of local and specific changes which can be very problematic to discuss. This approach, which is very common in analysis of many biological, physical and engineering systems, is most of the time very useful and can provide better results when compared to the more detailed models.

Based on the fitted phase parameters of cells, changes on the matching dielectric characteristics of the tagged cells were observed (Table 2). Those changes are well adapted to the cellular and molecular state of modified cells. The *lectin* coating on *MBA* cells was found to increase membrane permittivity. Here the membrane is more polar and hydrophilic comparing to the membrane of the untreated cells. The obtained relative permittivity values (*MBA-lectin* = 7.53, *MBA* = 6.11) are therefore representing those changes.

The cytoplasm conductivity of *MDCK-SEC13* cells was clearly affected by the over expression of *SEC13* protein. *SEC13* is known to be one of the most important proteins related to transport mechanism between the

Table 3
Relaxation and frequency characteristics of native and treated cell lines

Cell	τ_x(s)	f_x (MHz)	τ_y(s)	f_y(MHz)	τ_z(s)	f_z(MHz)
MBA	$3.3{\cdot}10^{-6}$	0.3	$4{\cdot}10^{-7}$	2.5	$2.4{\cdot}10^{-8}$	40.9
MBA-lectin	$5.9{\cdot}10^{-6}$	0.17	$7.1{\cdot}10^{-7}$	1.4	$3.4{\cdot}10^{-8}$	28.8
MDCK	$2.4{\cdot}10^{-6}$	0.41	$2.7{\cdot}10^{-7}$	3.7	$1.5{\cdot}10^{-8}$	67.3
MDCK-SEC13	$1.9{\cdot}10^{-6}$	0.52	$2.4{\cdot}10^{-7}$	4.1	$1.4{\cdot}10^{-8}$	70.9

ER (Endoplasmic Reticulum) and Golgi apparatus; its main activity is related to vesicles budding and release [39,40]. In cytoplasm, *SEC13* is found as part of hetrooligomery complex (150 kDa) [40]. Based on its molecular function, it seems reasonable that over expression of *SEC13* will lead to additional sub-expressions and formation of associate proteins related to this complex. Therefore, the net molecular charge in cytoplasm will also be affected by those products.

The obtained cytoplasm conductivity of *MDCK-SEC13* cells (9.98 ms/cm) is therefore partially affected from the above phenomenon, but it is not in contradiction to the fundamental finding regarding the more general change in cytoplasm conductivity when compared to the native cells (9.3 ms/cm).

The obtained differences in phase parameters of cells can be clarified through the use of equivalent three phase model, which describes the nature of relaxation in single-shell ellipsoid cell suspended in a conductive medium. Here, the induced dipole is strongly dependent on the electrical and structural properties of the components. Therefore, as direct consequence, the dispersion characteristics should be very sensitive to fine transformations occur within the system and can provide true knowledge regarding molecular and cellular changes occur on the cells.

At a low frequency the conductive polarization (charge migration) is dominant over dielectric polarization; therefore, the conductive charging of membrane is producing a large polarization across the membrane. When the frequency is increased such that it exceeds the inverse *RC* time of the polarized medium-membrane interface, field penetration into the cytoplasm interior will occur, resulting in dispersion (relaxation) that is governed by cytoplasm and medium conductivities.

The equivalent electric circuit of the above phenomena is modeled by a serial representation of three parallel *R–C* (resistor–capacitor) elements which represent the conductivity and permittivity of the medium, membrane and the cytoplasm [38,41]. Of course, this planner representation does not take into account the true structural geometry of the interfaces, and therefore, can only provide general estimation regarding the dominate elements at the described system. The relaxation time of the equivalent system is given by Eq. (10).

$$\tau = \frac{2\left(R_{\mathrm{med}}\tau_{\mathrm{mem}}\tau_{\mathrm{cyt}} + R_{\mathrm{mem}}\tau_{\mathrm{med}}\tau_{\mathrm{cyt}} + R_{\mathrm{cyt}}\tau_{\mathrm{med}}\tau_{\mathrm{mem}}\right)}{R_{\mathrm{med}}\left(\tau_{\mathrm{mem}} + \tau_{\mathrm{cyt}}\right) + R_{\mathrm{mem}}\left(\tau_{\mathrm{med}} + \tau_{\mathrm{cyt}}\right) + R_{\mathrm{cyt}}\left(\tau_{\mathrm{med}} + \tau_{\mathrm{mem}}\right)}, \quad \tau_i = R_i C_i \tag{10}$$

The thin dielectric membrane capacitance is given by $\varepsilon_{\mathrm{mem}}/d_{\mathrm{mem}}$ when $d_{\mathrm{mem}} \ll d_{\mathrm{cyt}}$, therefore, it is much higher than that of the cell interior. Since the membrane of biological cells is considered as low conductivity elements [35], the resistor component (R_{mem}) can be neglected (yields very high resistivity). The low conductive membrane is then assumed to be ideal insulating membrane. Therefore, the charge relaxation time (Eq. (11)) is then dependent on cytoplasm conductivity and membrane permittivity when the medium conductivity and permittivity are fixed parameters.

$$\tau \approx \frac{2R_{\mathrm{med}}R_{\mathrm{cyt}}\left(C_{\mathrm{med}}C_{\mathrm{mem}}\right)}{R_{\mathrm{med}}\left(C_{\mathrm{med}} + C_{\mathrm{mem}}\right) + R_{\mathrm{cyt}}C_{\mathrm{mem}}} \tag{11}$$

In order to define the exact relaxation time in ellipsoid cell systems, the permittivity equation for randomly oriented shelled-ellipsoid cell (Eq. (2)) can be modified to provide six Debye type relaxation terms (Eq. (12)) [38,42,43]. Of course, it should be assumed that both of the components (membrane and cytoplasm) are loss free, and also have well defined constant characteristics at the given frequency range. This assumption does not exclude the possibility that those components demonstrate dielectric loss in higher frequency range.

$$\varepsilon^* - \varepsilon_m^* = \sum_k \varepsilon_{hk} + \frac{\varepsilon_{lk1} - \varepsilon_{hk1}}{1 + j\omega\tau_{k1}} + \frac{\varepsilon_{lk2} - \varepsilon_{hk2}}{1 + j\omega\tau_{k2}} - j\frac{\tilde{\sigma}_k}{\omega\varepsilon_0}, \quad k{=}x,y,z \tag{12}$$

Here ε_{hk} is the limit of permittivity at high frequency, $\varepsilon_{lki}-\varepsilon_{hki}$ is the dispersion magnitude, τ_{ki} is the relaxation time, ω is the angular frequency and $\tilde{\sigma}_k$ is the dc conductivity at low frequencies. Based on Eqs. (12) and (2) and for low conducting and very thin membrane, the relaxation time across each axis can be given using a single term [45], when:

$$\tau_k \approx \frac{\varepsilon_0\varepsilon_{\mathrm{om}}\Phi}{\Delta_L}\left(\frac{R_xR_yR_z}{R_yR_z + R_xR_z + R_xR_y}\right)\left(\frac{1}{L_k\sigma_i} + \frac{1}{(1-L_k)\sigma_m}\right), \quad k = x,y,z \tag{13}$$

The relaxation term (Eq. (13)) is therefore in full agreement with the simple analog model described earlier. It demonstrates the strong dependency of the relaxation times in cytoplasm conductivity,

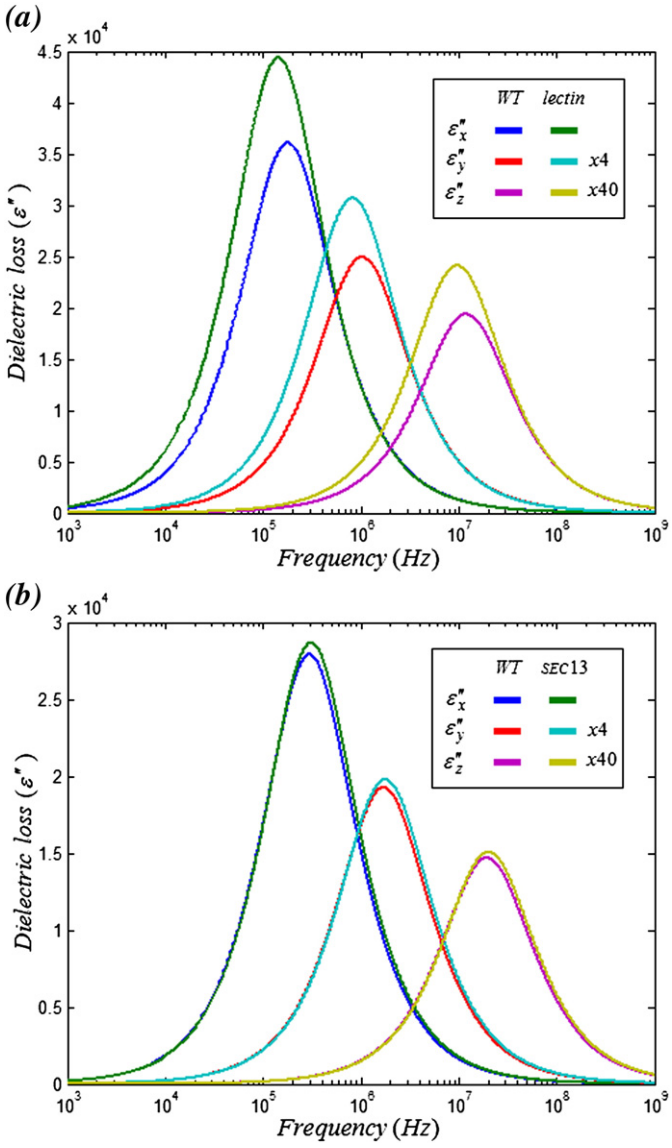

Fig. 7. Loss spectra of *MBA* and *MDCK* cells, here the losses are given by the *x, y, z* axes of cells. (a) Loss spectra of *MBA* and *MBA-lectin* cells. (b) Loss spectra of *MDCK* and *MDCK-SEC13* cells.

membrane permittivity and the structural morphology. Therefore, it can provide reliable indication regarding changes related to cell morphology and its molecular properties. The relaxation times and characteristic frequencies of both native and treated *MBA* and *MDCK* cell lines are summarized in Table 3. In addition, the dielectric loss spectra of cells are given in Fig. 7.

As suggested in the result section, both cell lines exhibit differences in relaxation times between *WT* and mutants (treated cells). Based on the fact that no changes occurred in the morphology of the cells, both differences can be attributed to changes occurred on cytoplasm conductivity and membrane permittivity which affected the conductive relaxation of cells. The increase of relaxation times in *MBA-lectin* tagged cells is attributed to the rise of membrane permittivity. Here the charging effect caused by *lectin* antibodies, increased the membrane capacitance, and hence, increased the relaxation times of cells. The opposite affect is observed in *MDCK* cell lines. Here the over expression of *SEC13* protein increased cytoplasm conductivity (resistivity decreased) and hence, the relaxation times found to be lower as expected.

The equivalent loss plots (Fig. 7) indeed support those finding. Here the characteristic frequencies found to be slightly shifted according to the changes occurred in relaxation times of both cells. Those changes are directly attributed to the differences occurred in dielectric characteristics of the treated cells (*MBA-lectin, MDCK-SEC13*) comparing to native ones.

6. Conclusions

The high sensitivity of DS, as demonstrated here and by other in the past [4–7, 13–16, 44–47], has promise potential as a screening tool on live cell libraries. It can be used for quantitative and systematic analysis on multiple micro-libraries labeled with specific probes in non invasive and non destructive way. It can also allow real time screening after fine biochemical effects on both cellular and molecular level, which cannot be detected using traditional screening assays.

Here, target identification of specific cellular phenotypes was demonstrated using dielectric screening method. Using the fundamentals of mixed dielectric theories, the electric properties of cells were determined by fitting the well established shelled-ellipsoid model into the measured spectra. Those unique properties found to be well adapted to the molecular and structural state of the analyzed cells. In addition, the dispersion characteristics found to be with full agreement with the molecular state of the cells which supports the findings presented here.

However, and without casting doubt on the reported results, the presented work should only provide general knowledge regarding the use of DS as potential screening tool. All the results should be considered as preliminary especially in the case of cytoplasmatic tagging, when minute and fine changes are observed, comprehensive and deeper analysis should be performed in order to reinforce the presented findings.

List of symbols

R_x, R_y, R_z Semi axes of cell.
R_{ix}, R_{iy}, R_{iz} Semi axes of cytoplasm.
Δ_L Thickness of phospholipids membrane.
N Number of cells.
Φ Volume fraction of cells.
ε_m^* Relative permittivity of external medium, when: $\varepsilon_m^* = \varepsilon_m' - j\varepsilon_m'' = \varepsilon_m' - j\sigma_m/(\omega\varepsilon_0)$.
ε_{om}^* Relative permittivity of membrane, when: $\varepsilon_{om}^* = \varepsilon_{om}' - j\varepsilon_{om}'' = \varepsilon_{om}' - j\sigma_{om}/(\omega\varepsilon_0)$.
ε_i^* Relative permittivity of cytoplasm, when: $\varepsilon_i^* = \varepsilon_i' - j\varepsilon_i'' = \varepsilon_i' - j\sigma_i/(\omega\varepsilon_0)$.
ε_0 Permittivity of free space $= 8.85 \cdot 10^{-12}\ C^2/Nm^2$.
med External medium.
mem Membrane.
cyt Cytoplasm.
d Thickness.
$\tau_{med} = R_{med}C_{med}$ Analog relaxation time of medium.
$\tau_{mem} = R_{mem}C_{mem}$ Analog relaxation time of membrane.
$\tau_{cyt} = R_{cyt}C_{cyt}$ Analog relaxation time of cytoplasm.

Acknowledgements

CellProm project, FP6th of the European Community (NMP4-CT-2004-500039).

References

[1] R. Hoeber, Eine Methode die elektrische Leitfaehigkeit im Innern von Zellen zu messen, Arch. ges. Physiol. 133 (1910) 237–259.
[2] H.P. Schwan, T.P. Bothwell, F.J. Wiercinski, Electrical properties of beef erythrocyte suspensions at low frequencies, Fed. Proc. Am. Soc. Exp. Biol. 13 (1954) 15–16.
[3] H.P. Schwan, T.P. Bothwell, Electrical properties of the plasma membrane of erythrocytes at low frequencies, Nature 178 (1956) 265–266.
[4] A. Surowice, S.S. Stuchly, C. Izaguirre, Dielectric properties of human B and T lymphocytes at frequencies from 20 kHz to 100 MHz, Phys. Med. Biol. 31 (1986) 43–53.
[5] K. Asami, Y. Takahashi, S. Takashima, Dielectric properties of mouse lymphocytes and erythrocytes, Biochem. Biophys. Acta 1010 (1989) 49–55.
[6] F. Bordi, C. Cametti, A. Rosi, A. Calcabrini, Frequency domain electrical conductivity measurements of the passive electrical properties of human lymphocytes, Biochem. Biophys. Acta 1153 (1993) 77–88.
[7] H. Beving, L.E.G. Eriksson, C.L. Davey, D.B. Kell, Dielectric properties of human blood and erythrocytes at radio frequencies (0.2–10 MHz); dependence on cell volume fraction and medium composition, Eur. Biophys. J. 23 (1994) 207–215.
[8] K.R. Foster, H.P. Schwan, Dielectric properties of tissues and biological materials: a critical review, Crit. Rev. Biomed. Eng. 17 (1989) 25–104.
[9] E.H. Grant, R.J. Sheppard, G.P. South, Dielectric Behaviour of Biological Molecules in Solutions, Clarendon Press, Oxford, 1978.
[10] S. Takashima, Electrical Properties of Biopolymers and Membranes, Institute of Physics Publishing, Philadelphia, 1989.
[11] E.H. Grant, Electrical behaviour of egg albumen solutions at ultra-high frequencies, Nature 196 (1962) 1194–1195.
[12] S.E. Keefe, E.H. Grant, Dipole moment and relaxation-time of ribonuclease, Phys. Med. Biol. 19 (1974) 701–707.
[13] K. Asami, Effect of cell shape on dielectric behaviour of fission yeast, Biochem. Biophys. Acta 1472 (1999) 137–141.
[14] K. Asami, T. Hanai, Dielectric monitoring of biological cell sedimentation, Colloid Polym. Sci. 270 (1992) 78–84.
[15] A. Irimajiri, M. Ando, R. Matsuoka, T. Ichinowatari, S. Takeuchi, Dielectric monitoring of rouleaux formation in human whole blood: a feasibility study, Biochim. Biophys. Acta 1290 (1996) 207–209.
[16] K. Asami, E. Gheorghiu, T. Yonezawa, Real-time monitoring of yeast cell division by dielectric spectroscopy, Biophys. J. 76 (1999) 3345–3348.
[17] V. Raicu, T. Saibara, H. Enzan, A. Irimajiri, Dielectric properties of rat liver in vivo: analysis by modeling hepatocytes in the tissue architecture, Bioelectrochem. Bioenerg. 47 (1998) 333–342.
[18] K. Asami, A. Irimajiri, Dielectrospectroscopic monitoring of early embryogenesis in single frog embryos, Phys. Med. Biol. 45 (2000) 3285–3297.
[19] H. Frick, A Mathematical treatment of the electric conductivity and capacity of disperse systems I. The electric conductivity of a suspension of homogeneous spheroids, Phys. Rev. 24 (1924) 575–587.
[20] H. Frick, The electric permittivity of a dilute suspension of membrane-covered ellipsoids, J. Appl. Phys. 24 (1953) 644–646.
[21] H. Pauly, H.P. Schwan, Uber die Impedanz einer suspension von kugelformigen teilchen mit einer schale, Z. Naturforsch. 14 (1959) 125–131.
[22] T. Hanai, N. Koizumi, A. Irimajiri, A method for determining the dielectric constant and the conductivity of membrane-bounded particles of biological relevance, Biophys. Struct. Mech. 1 (1975) 285–294.
[23] W.R. Redwood, S. Takashima, H.P. Schwan, T.E. Thompson, Dielectric studies on homogeneous phosphatidylcholine vesicles, Biochim. Biophys. Acta 255 (1972) 557–566.
[24] K. Asami, T. Hanai, N. Koizumi, Dielectric approach to suspensions of ellipsoidal particles covered with a shell in particular reference to biological cells, Jpn. J. Appl. Phys. 19 (1980) 359–365.
[25] J. Shepshelovich, K. Hirschberg, Expression, localization, and topology of fluorescently tagged plasma membrane-targeted transmembrane proteins, Methods Mol. Biol. 390 (2007) 393–404.
[26] D. Benayahu, Y. Kletter, D. Zipori, S. Wientroub, Bone marrow-derived stromal cell line expressing osteoblastic phenotype in vitro and osteogenic capacity in vivo, J. Cell Physiol. 140 (1989) 1–7.
[27] I. Shur, R. Marom, F. Lokiec, R. Socher, D. Benayahu, Identification of cultured progenitor cells from human marrow stroma, J. Cell. Biochem. 87 (2002) 51–57.
[28] B. Ilic, D. Czaplewski, P. Neuzil, T. Stanczyk, J. Blough, G.J. Maclay, Preparation and characterization of platinum black electrodes, J. Mater. Sci. 35 (2000) 3447–3457.
[29] S. Darayan, D. Shattuck, L. Shen, C. Liu, Measurement of dielectric constant and conductivity of samples using guarded electrode, Radio Sci. 31 (1996) 1417–1426.

[30] B. Onaral, H.P. Schwan, Linear and nonlinear properties of platinum electrode polarisation. Part 1: frequency dependence at very low frequencies, Med. Biol. Eng. Comput. 20 (1982) 299–306.
[31] H.P. Schwan, Alternating current electrode polarization, Biophysik 3 (1966) 181–201.
[32] H.P. Schwan, Linear and nonlinear electrode polarization and biological materials, Ann. Biomed. Eng. 20 (1992) 269–288.
[33] H.P. Schwan, Physical Techniques in Biological Research, vol. VI, Academic Press, 1963, pp. 323–407.
[34] V. Raicu, G. Raicu, G. Turcu, Dielectric properties of yeast cells as simulated by the two-shell model, Biochim. Biophys. Acta 1274 (1996) 143–148.
[35] D. Johnston, S. Miao-Sin Wu, Foundations of Cellular Neurophysiology, MIT press, 1995.
[36] J. Lärmer, S.W. Schneider, T. Danker, A. Schwab, H. Oberleithner, Imaging excised pical plasma membrane patches of *MDCK* cells in physiological conditions with atomic force microscopy, Eur. J. Physiol. 434 (1997) 254–260.
[37] J.T. Elliott, A. Tona, J.T. Woodward, C.W. Meuse, H.M. Elgendy, A.L., Plant osteoblast cell membrane hybrid bilayers for studying cell–cell interactions, IEEE Proc. Nanobiotechnol. 151 (2004) 75–81.
[38] K. Asami, Characterization of heterogeneous systems by dielectric spectroscopy, Prog. Polym. Sci. 27 (2002) 1617–1659.
[39] D.A. Shaywitz, et al., Human SEC13Rp functions in yeast and is located on transport vesicles budding from the endoplasmic reticulum, J. Cell Biol. 128 (1995) 769–777.
[40] N.R. Salama, T. Yeung, R.W. Schekman, The Secl3p complex and reconstitution of vesicle budding from the ER with purified cytosolic proteins, EMBO J. 12 (1993) 4073–4082.
[41] L.K.H. van Beek, Dielectric behaviour of heterogeneous systems, Prog. Dielectr. 7 (1967) 69–117.
[42] P. Debye, Polar Molecules, Dover Publications, New York, 1929.
[43] K. Asami, T. Yonezawa, Dielectric behaviour of non spherical cells in culture, Biochem. Biophys. Acta 1245 (1995) 317–324.
[44] Y. Feldman, I. Ermolina, Y. Hayashi, Time domain dielectric spectroscopy study of biological systems, Trans. Dielect. Electr. Insul. 10 (2003) 728–753.
[45] Y. Polevaya, I. Ermolina, M. Schlesinger, B.Z. Ginzburg, Y. Feldman, Time domain dielectric spectroscopy study of human cells. II. Normal and malignant white blood cells, Biochem. Biophys. Acta 1419 (1999) 257–271.
[46] I. Erimolina, Y. Polevaya, Y. Feldman, Analysis of dielectric spectra of eukariotic cells by computer modeling, Eur. Biophys. J. 29 (2000) 141–145.
[47] C. Prodan, F. Mayo, J.R. Claycomb, J.H. Miller, Low-frequency, low-field dielectric spectroscopy of living cell suspensions, J. Appl. Phys. 95 (2004) 3754–3756.